

## THE DYNAMICS OF STAR STREAM GAPS

R. G. CARLBERG

Department of Astronomy and Astrophysics, University of Toronto, Toronto, ON M5S 3H4, Canada  
*Draft version June 26, 2018*

### ABSTRACT

When a massive object crosses a star stream velocity changes are induced both along and transverse to the stream which can lead to the development of a visible gap. For a stream narrow relative to its orbital radius the time of stream crossing is sufficiently short that the impact approximation can be used to derive the changes in angular momenta and radial actions along the star stream. The epicyclic approximation is used to calculate the evolution of the density of the stream as it orbits around in a galactic potential. Analytic expressions are available for a point mass, however, the general expressions are easily numerically evaluated for perturbing objects with arbitrary density profiles. With a simple allowance for the velocity dispersion of the stream, moderately warm streams can be modeled. The predicted evolution agrees well with the outcome of simulations of stellar streams for streams with widths up to 1% of the orbital radius of the stream. The angular momentum distribution within the stream shears out gaps with time, further reducing their visibility, although the size of the shear effect requires more detailed simulations. An illustrative model indicates that shear will limit the persistent gaps to a minimum length of a few times the stream width. In general the equations are useful for dynamical insight into the development of stream gaps and their measurement.

*Subject headings:* dark matter; Galaxy: structure; Galaxy: kinematics and dynamics

### 1. INTRODUCTION

Star streams are created as the gravitational field of the galaxy tidally disrupts a dwarf galaxy or globular star cluster orbiting in the halo of a galaxy. Streams will exhibit a rich range of features along their length as a result of variations in the gravitational field. A progenitor in any non-circular orbit will experience varying tidal fields around the orbit, leading to an increased mass loss rate near perigalacticon (Dehnen et al. 2004). As the unbound stream stars orbit they bunch up at apogalacticon and spread out at perigalacticon (Johnston 1998; Johnston et al. 2001). Stars leave the progenitor near the inner and outer Lagrange points where unbound stars are roughly collimated into a radial outward stream which leads to regular cycloidal density variations near the beginning of the stream (Küpper et al. 2008, 2010, 2012). Finally, within an LCDM dark matter halo there are predicted to be large numbers of dark matter sub-halos (Diemand, Kuhlen & Madau 2007; Springel et al. 2008; Stadel et al. 2009) with  $n(M) dM \propto M^{-1.9} dM$ . The sub-halos induce gaps when they cross a star stream (Yoon, Johnston & Hogg 2011; Carlberg 2009, 2012).

Although gaps are purely a statistical measure of the dark matter sub-halo population they do have the attractive property that the individual cross-section depends on their radius,  $R \propto M^{0.43}$ , which means that the cross-section for gap creation integrated over the sub-halo population,  $A(M) n(M) dM$ , is dominated by the smallest masses that can create a visible gap. The dominance of the low mass members of the population is useful in discriminating between cold and some forms of warm dark matter, where warm dark matter has very few sub-halos below  $\sim 10^{8-9} M_{\odot}$  for a 1 Kev dark matter particle (Barkana et al. 2001; Bode et al. 2001; Benson et al. 2013; Angulo et al. 2013; Schneider et al. 2013).

In this paper we develop the general expressions for the changes in velocities as a result of the passage of massive object. We re-derive the result of Yoon, Johnston & Hogg (2011) for the velocity change along the stream and present the result perpendicular to the stream. We use the general expressions for an arbitrary mass density profile to derive the changes for a stream on a galactic orbit and the resulting evolution of density along the stream. Adding a dispersion in angular momentum and radial action allows for the finite width of streams. The predictions are then compared to velocity changes and gaps in simulations.

### 2. RESPONSE OF THE STREAM STARS TO AN ENCOUNTER

We make a few assumptions to simplify the analysis of the encounter between a massive object and a stream of stars. First, we assume that the encounter is sufficiently fast and weak that the changes in the star stream velocities are small relative to their orbital velocities, *i.e.*, the impact approximation. Second, we will do the basic analysis for a zero initial width stream. However, we will show that the results are applicable to streams of finite width with random velocities and shear velocities. And third, we assume that the orbit of the stream is circular in an axisymmetric potential. In a non-circular orbit there will be an additional systematic compression and extension of the stream and the features within it around the orbit.

#### 2.1. Velocity Changes of the Stars

The epicyclic approximation expands about an orbit of constant angular momentum,  $J_{\phi}$ , where  $\phi$  is the angle around a circular orbit. The local co-ordinate system for our analysis is shown in Figure 1. A Cartesian frame with the  $x$  coordinate is aligned in the radial direction (Binney & Tremaine 2008) measured from the center of

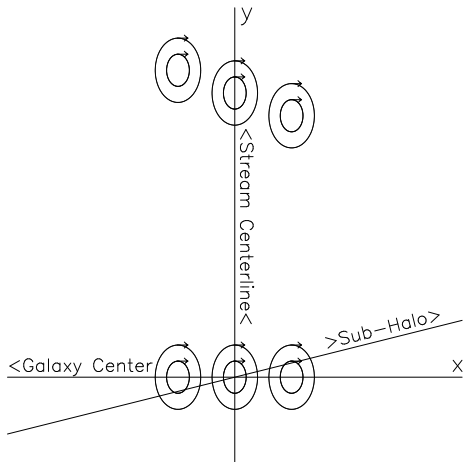


FIG. 1.— The coordinate system for the analysis and the basic motions. The stream moves upward at velocity  $v_y$  along the  $y$  axis with the  $t = 0$  value of  $y$  being used to label the stars. The sub-halo crosses the  $x$ -axis at  $[b_x, 0, b_z]$  at  $t = 0$  with a velocity  $[V_x, V_y, V_z]$ . The epicycles rotate opposite to the stream rotation around the galaxy. The angular velocity decreases outwards so stars with guiding centers at larger radii fall behind those at smaller radii.

the progenitor. The stream then moves in the positive  $y$  direction. Stars with the same angular momentum share a common guiding center radius, but differences in radial velocity lead to different size epicycles around the guiding center. Stars with larger angular momentum have a larger guiding center radius where the rate of angular rotation is lower, so stars initially aligned at the same  $y$  but at different  $x$  will gradually shear with respect to each other as they move forward along the  $y$  axis at different rates.

The section of the stream that interacts most strongly with a passing sub-halo is a few times the sub-halo's scale radius (Carlberg 2012). For sub-halos of  $10^8 M_\odot$  the scale radius is about 0.8 kpc so the interaction region for a sub-halo orbiting in the halo beyond the disk is normally sufficiently small relative to the orbital radius that the response to the perturbation can be calculated as if the stream were a straight line. The coordinate distances between the stream stars moving at a uniform velocity  $v_y$  and a sub-halo moving at velocity  $[V_x, V_y, V_z]$  which crosses  $y = 0$  at time  $t = 0$  is,

$$\vec{d}(y, t) = [b_x + V_x t, y + (v_y - V_y)t, b_z + V_z t], \quad (1)$$

where  $y$  is the  $t = 0$  location of stars along the stream and the closest approach distance  $b$  is resolved into its  $x$  and  $z$  components. A perturbing mass with a spherically symmetric gravitational potential  $\Phi(r)$ , induces a net velocity change along the stream of,

$$\Delta \vec{v}(y) = - \int_{-\infty}^{\infty} \vec{\nabla} \Phi(|\vec{d}(y, t)|) dt. \quad (2)$$

Equations 2 are straightforward to numerically integrate for most radially symmetric density profiles.

To illustrate the behavior of these equations the velocity changes of Equations 2 can be analytically integrated for a perturbing point mass,  $M$ . We define the velocity of the point mass relative to the stream,  $v_{\parallel} = v_y - V_y$  and orient the  $x - z$  frame so that  $v_{\perp}$  is the velocity to-

ward the stream,  $\sqrt{V_x^2 + V_z^2}$ . The impact parameter is  $b = \sqrt{b_x^2 + b_z^2}$ .

The substitutions allow the integral of Equation 2 for the component of the velocity change parallel to the stream motion for the point mass to be written as,

$$\Delta v_{\parallel}(y) = \int_{-\infty}^{\infty} \frac{-GM (v_{\parallel} t + y)}{[v_{\perp}^2 t^2 + (v_{\parallel} t + y)^2 + b^2]^{3/2}} dt. \quad (3)$$

Doing the integral of Equation 3 gives the change in the  $v_{\parallel}$  component of the stream stars is,

$$\Delta v_{\parallel}(y) = \frac{-2GM v_{\perp}^2 y}{v (v^2 b^2 + v_{\perp}^2 y^2)}, \quad (4)$$

where  $v = \sqrt{v_{\parallel}^2 + v_{\perp}^2}$  is the speed of the perturbing mass relative to the stream stars. This equation has been previously derived in Yoon, Johnston & Hogg (2011) with slightly different notation.

Perpendicular to the stream the velocity change is,

$$\Delta v_{\perp}(y) = \int_{-\infty}^{\infty} \frac{-GM v_{\perp} t}{[v_{\perp}^2 t^2 + (v_{\parallel} t + y)^2 + b^2]^{3/2}} dt, \quad (5)$$

which integrates to,

$$\Delta v_{\perp}(y) = \frac{2GM v_{\perp} v_{\parallel} y}{v (v^2 b^2 + v_{\perp}^2 y^2)}. \quad (6)$$

Equation 6 is non-zero along the stream only in the special case that  $v_{\parallel} = 0$ .

It is interesting to note that the ratio of Equations 4 and 6 is,

$$\frac{\Delta v_{\perp}(y)}{\Delta v_{\parallel}(y)} = -\frac{v_{\parallel}}{v_{\perp}}. \quad (7)$$

The ratio of the two velocity perturbations does not depend on distance along the stream or impact parameter, only on the velocity of the perturbing mass relative to the stream. We note that since  $v_{\parallel}$  is the relative velocity in the stream direction of the perturber and the stream stars it can be small and even change sign.

## 2.2. Orbital Changes and Stream Gaps

The stream is orbiting within a galaxy, hence the response of the stream to the perturbing mass needs to be placed within the framework of orbital dynamics. For simplicity we continue to assume that the stream is on a circular orbit at a radius  $X_0$ . The relation between the linear coordinate  $y$  and the  $t = 0$  angular coordinates,  $\phi(0)$ , is simply  $y = \phi(0)X_0$ . The velocity change parallel to the motion of the stream,  $\Delta v_{\parallel}(y)$ , are changes in the angular momentum,  $J_{\phi}$ , of the stream stars. For small ellipticity orbits the epicyclic approximation gives the angular momentum as  $J_{\phi} = X v_c$ , where  $X$  is the guiding center radius and  $v_c(X)$  is the circular velocity. The guiding center rotates forward at a uniform rate  $\Omega(X)$ . The epicycle is centered on the guiding center, with the star traveling around the elliptical epicycle in the opposite direction to the mean angular rotation at a rate  $\kappa(X)$  (Binney & Tremaine 2008). After the encounter with a sub-halo the angular momentum along the stream is,

$$J_{\phi}(y) = v_c(X_0)X_0 + \Delta v_{\parallel}(y)X_0, \quad (8)$$

where  $X_0$  is the pre-encounter guiding center radius. The angular momentum changes lead to new guiding centers along the stream,

$$X = X_0 \frac{v_c(X_0) + \Delta v_{\parallel}(y)}{v_c(X)}. \quad (9)$$

Consequently, after the encounter the stars move at angular rates that are a function of their new guiding centers,  $\Omega = v_c/X$ , or,

$$\Omega(y) = \frac{v_c}{X_0} \left[ 1 + \frac{\Delta v_{\parallel}(y)}{v_c} \right]^{-1}, \quad (10)$$

where we have assumed for simplicity that  $v_c$  is locally constant, although the result can be generalized to any rotation curve shape using a linear expansion. An acceleration forward leads to the stars rotating more slowly and vice-versa, which opens up a gap in the star stream centered on  $y = 0$ , the crossing point of the sub-halo.

### 2.2.1. The Gap Density Profile

The length and approximate density profile of a gap are readily calculated from the perturbed motion of the stars. The linear density along the stream is  $\rho \equiv X_0^{-1} dn/d\phi$ . After the encounter the stars in the stream are at angles  $\phi(t) = \phi + \Omega(\phi X_0)t$ . Therefore the differential in the density equation becomes,

$$d\phi(t) = \left( 1 + X_0 \frac{d\Omega(y)}{dy} t \right) d\phi. \quad (11)$$

Using Equation 10 in Equation 11 the linear density along the stream becomes,

$$\rho(y, t) = \rho_0 \left[ 1 - \left( 1 + \frac{\Delta v_{\parallel}(y)}{v_c} \right)^{-2} \frac{d\Delta v_{\parallel}(y)}{dy} t \right]^{-1}. \quad (12)$$

In principle one could allow for streams on non-circular orbits by including the variation of  $\Omega(r)$ .

Equation 12 gives the density as a function of time, labeled with the initial  $y$  values. The gap has its greatest depth at  $y = 0$ , where Equation 4 gives  $\Delta v_{\parallel} = 0$  its derivative is always negative for reasonable perturbing mass profiles. Therefore the density in the gap goes to zero asymptotically as  $t^{-1}$ . On either side of the gap where  $d\Delta v_{\parallel}(y)/dy > 0$  Equation 12 will fail for sufficiently large  $t$  values that the expression in brackets goes through zero and becomes negative.

As the guiding centers change in response to the angular momentum changes, the mean orbital angle at which the density applies is modified from the pre-encounter  $\phi(t) = y/X_0 + \Omega_0 t$ , to,

$$\phi(y, t) = \frac{y}{X_0} + \Omega(y)t, \quad (13)$$

where we use the  $\Omega(y)$  of Equation 10 to give the result. Equation 13 ignores the epicyclic oscillations of individual stars, on the basis that this oscillating term will normally average to zero in a realistic stream that contains random motions. Equation 13 is the angle relative to the current location of the middle of the gap. Subtracting the gap center angular rotation of  $v_c/X_0$  from the  $\Omega(y)$  of Equation 10 removes the mean motion to give

$\Delta\phi(y, t) = \phi(y, t) - v_c/X_0$ , which when into Equation 13 gives,

$$\Delta\phi(y, t) = \frac{y}{X_0} - \frac{v_c}{X_0} \frac{\Delta v_{\parallel}(y)}{v_c} \left[ 1 + \frac{\Delta v_{\parallel}(y)}{v_c} \right]^{-1} t. \quad (14)$$

Equations 12 and 14 are parametric equations in the density,  $\rho(y, t)$  and angle  $\Delta\phi(y, t)$  with  $y$  and  $t$  as parameters.

The density in the stream, Equation 12, develops a gap in the region where  $d\Delta v_{\parallel}/dy$  is negative. For the point mass object,

$$\frac{d\Delta v_{\parallel}}{dy} = -\frac{2v_{\perp}^2 GM(v^2 b^2 - v_{\perp}^2 y^2)}{v(v^2 b^2 + v_{\perp}^2 y^2)}. \quad (15)$$

Therefore the stream will have a density reduction over an interval of length given by the locations of the zeros of  $d\Delta v_{\parallel}/dy$ , or  $y = \pm v/v_{\perp} b$  at time  $t = 0$  of Equation 13. Equation 10 gives the second term of Equation 13. The time development of the gap length in our point mass example then is,

$$\ell(t) = \frac{2b}{X_0} \left( \frac{v}{v_{\perp}} + \frac{v^2}{v^2 b + GM v_{\perp}} v_c t \right). \quad (16)$$

The gap grows linearly with time from its post-encounter initial size, which in reality takes about an orbital period to develop. The gap that the extended mass profile of a sub-halo induces will have a similar character although the detailed functional form of the gap will depend on the mass profile of the perturber.

### 2.2.2. Changes of Epicyclic Motions

We are also interested in the changes in the sizes of the epicycles. For an epicycle of radial extent  $a$ ,  $x(t) = a \cos(\kappa t + \psi)$ , and the velocity  $\dot{x}(t) = -\kappa a \sin(\kappa t + \psi)$  where  $a$  and  $\psi$  are the amplitude and orbital phase, respectively, of the epicycle. In the direction of the mean motion the epicyclic velocity is  $\dot{y}(t) = -2\Omega a \cos(\kappa t + \psi)$  (Binney & Tremaine 2008). The epicycle is an ellipse, with axes in the ratio  $2\Omega/\kappa$ .

An encounter with an initially completely cold stream will induce a systematic epicyclic motion through the combined effects of the velocity changes along and perpendicular to the stream. The radial motion immediately after the encounter is  $\Delta v_{\perp}(y)$ . Along the stream there is a velocity change of  $\Delta v_{\parallel}(y)$  to which we need to add the effective velocity change which results from the change to the new guiding center, Equation 9. The change of mean guiding center leads to an angular velocity difference between the initial orbits and the post-encounter orbit which is simply the initial angular velocity,  $v_c/X_0$ , minus the new angular rotation rate,  $\Omega(y)$ , of Equation 10. Expanding Equation 10 to first order and multiplying by the radius to get a linear velocity we find a second velocity change factor of  $\Delta v_{\parallel}(y)$ . Therefore, to first order the new velocity along the stream, in the frame of the new guiding center is  $2\Delta v_{\parallel}(y)$ . Since  $v_x/\kappa = a \sin(\kappa t + \psi)$  and  $v_y/(2\Omega) = a \cos(\kappa t + \psi)$ , the resulting added epicycle has a size in terms of the stream perturbations of,

$$a(y) = \sqrt{\frac{\Delta v_{\perp}^2(y)}{\kappa^2} + \frac{\Delta v_{\parallel}^2(y)}{\Omega^2}}. \quad (17)$$

The initial epicyclic phase,  $\psi$ , as a function of the stream position of this induced epicycle can be derived from the ratio of the two velocities at  $t = 0$ ,

$$\tan(\psi(y)) = \frac{2\Omega\Delta v_{\perp}(y)}{\kappa\Delta v_{\parallel}(y)}. \quad (18)$$

In a warm stream the pre-encounter epicycles will have random phases which the sub-halo induced epicycle will add leading to a spread in change in epicyclic size. Because the added epicyclic phase is coherent along the stream the stars will oscillate in and out together, with the stream varying from nearly straight, to a sideways reversed “S” shape.

### 3. COMPARISON TO IDEALIZED SIMULATIONS

#### 3.1. Simulation Setup

Running some simple gravitational simulations of a star stream orbiting in a galactic potential that encounters a sub-halo with an extended mass profile tests the accuracy and the generality of the analytic predictions. The galactic potential is an NFW halo (Navarro et al. 1997) with the peak of the rotation curve at 30 kpc where the circular velocity is  $210 \text{ km s}^{-1}$  that is a rough match to the dark halo of the Milky Way (Springel et al. 2008) although those details are not important for this illustrative calculation. The radius and mass define a characteristic mass of  $3.077 \times 10^{11} M_{\odot}$ , which together give a set of characteristic scales to normalize the numerical calculation units.

We place 100,000 particles on an arc of length 1 radian on a circular orbit at 30 kpc with velocities equal to the local circular velocity. The arc is positioned so that a perturbing sub-halo will cross the middle of the stream. Restricting attention to circular orbits is not a significant limitation for the relatively small size of the gaps that sub-halos induce, although the gap size and density will expand and contract to conserve angular momentum if the stream is on a non-circular orbit. One version of the stream is completely cold with all particles having the same angular momentum, no radial velocities and no initial width about the stream centerline. To understand the extension to warm streams with a finite width we also set up streams with a Gaussian distribution of epicycles about the same initial guiding centers. All the particles have the same angular momentum to first order, so there is no shear in the stream. This allows direct comparison with the model predictions above, but will need to be taken into account for comparison to real streams. In the warm simulations the epicycles are sufficiently small, generally less than 1% of the orbital radius, that the asymmetric drift correction to the mean orbital velocity, which is a second order effect, is ignored.

A sub-halo with a Hernquist mass profile having a mass of  $10^6 M_{\odot}$ , unless otherwise specified, is sent on a straight line orbit towards the stream at a constant velocity of  $1.2v_c$ . The simulation is initiated with the sub-halo at a distance of one stream radius away from where it will cross the stream at  $y = 0$  at time zero. The predictions for  $\Delta v_{\parallel}(y)$  and  $\Delta v_{\perp}(y)$  are worked out with the integrals of Equation 2. The results are only very weakly dependent on the precise angle with respect to the orbital plane with which the sub-halo encounters the stream, but there are differences of detail.

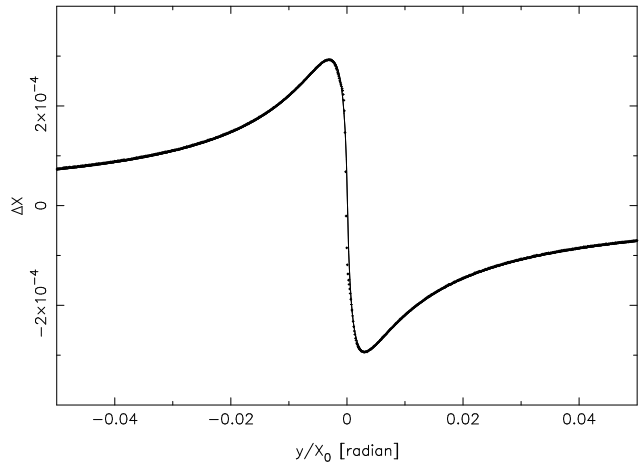


FIG. 2.— The changes in the guiding center radius, normalized to 30 kpc, after an encounter with a  $10^6 M_{\odot}$  sub-halo on a cold stream as a function of the pre-encounter co-ordinate along the stream. The impact parameter is 3 pc whereas the sub-halo has a scale radius of about 100 pc. The line shows the predicted relation, which is nearly indistinguishable from the simulation points.

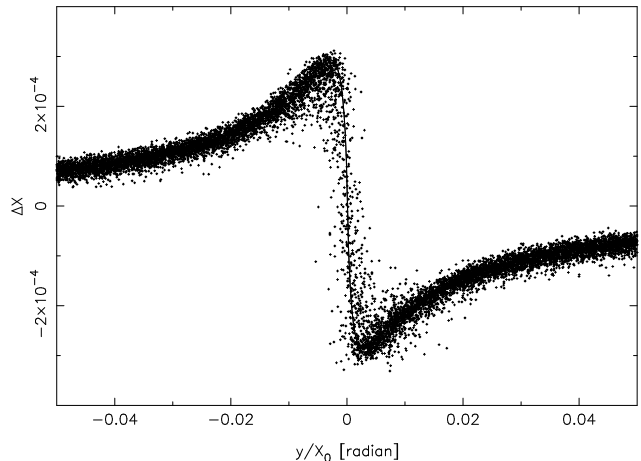


FIG. 3.— Same as Figure 2, but for a stream of width 0.23% of the orbital radius, equivalent to 70 pc.

We consider the response of completely cold and warm streams on circular orbits to a sub-halo of mass  $10^6 M_{\odot}$  with a Hernquist mass profile having a scale radius of 110 pc. For most encounters the impact parameter is set to 0.0001 of the orbital radius, that is, 3 pc, which is effectively a direct hit on the stream. The mass of  $10^6 M_{\odot}$  is chosen on the basis of being a sufficiently small mass that the linear approximations in the analysis should in principle give good descriptions of the dynamics. A significantly smaller sub-halo mass would have a size scale smaller than the narrowest streams and of less practical interest since the gap may be too shallow to be readily visible. The steep LCDM mass spectrum of sub-halos,  $N(M) \propto M^{-1.9}$  means that there should be large numbers at these masses ensuring that real streams will have many encounters with masses in this range.

The first simulated stream is completely cold and well matched to the assumptions of our analysis. The stream is warm with a width of 70 pc, the width of the GD-1 star stream (Carlberg & Grillmair 2013), or 0.23% of the or-

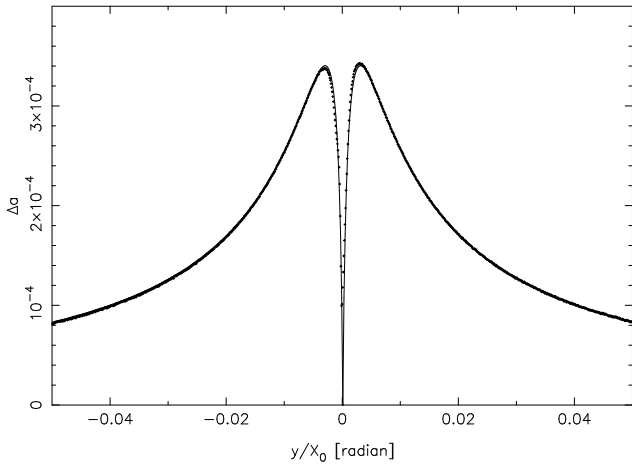


FIG. 4.— The changes in the calculated epicycle size, normalized to 30 kpc, for the cold stream simulation of Figure 2. The line shows the predicted relation which is nearly indistinguishable from the simulation points. In this case the sub-halo is shot from the outside in. There is a slight asymmetry of the two peaks in the simulation results.

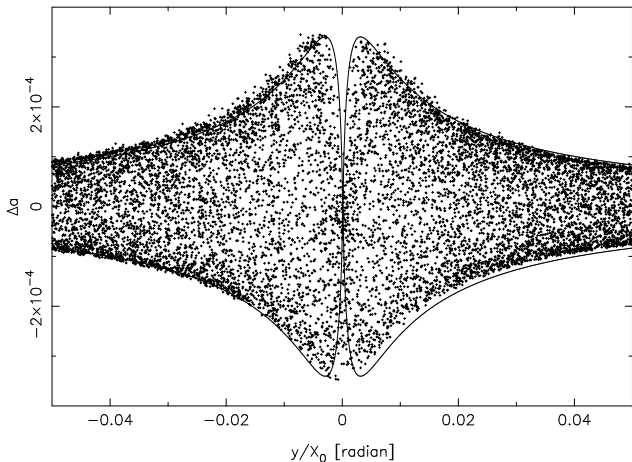


FIG. 5.— The change in epicycle sizes for a warm stream of width 70 pc. In this case the prediction of Equation 17 is shown as  $\pm a(y)$ .

bitual radius and is still very thin. A yet wider stream will be used to see where the approximations of our analysis begin to lead to significant quantitative errors.

### 3.2. Position and Velocity Changes in the Stream

Figure 2 shows the change in guiding center,  $\Delta X = X - X_0$  for the cold stream along with the predicted relation of Equation 9, integrated for the Hernquist potential used for the sub-halo in the simulation. The prediction is virtually indistinguishable from the simulation points. Figure 3 shows the same prediction against the post-encounter guiding centers calculated from the angular momentum values in a 70 pc wide stream. In this case there is a spread of values around the prediction, which we attribute to the fact that in a warm stream the individual stars have a range of velocities relative to the sub-halo, which leads to a range of relative  $v_{\parallel}$  and  $v_{\perp}$  for individual particles. For yet warmer streams (not shown) there is even more scatter and the angular momentum changes can even reverse sign, as anticipated in

our analytic results for the point mass object, Equation 7.

The change in the sizes of the epicycles,  $\Delta a = a - a_0$ , where  $a$  and  $a_0$  are the post encounter and initial epicyclic sizes, respectively, are compared to the prediction of Equation 17 for the cold stream (where  $a_0 = 0$ ) in Figure 4 showing that the prediction is quite good. The height of the two peaks in the  $\Delta a$  distribution in the simulation are slightly asymmetric whereas the prediction is completely symmetric about the center point. To identify the source of the asymmetry some variants on the basic simulation were done. The plot of Figure 4 uses a sub-halo started at twice the orbital radius and was shot inward. We repeated the simulation with the sub-halo shot outward from the center, finding that the asymmetry reverses and become stronger. The time evolution of  $\Delta a$  shows that before the sub-halo arrives at the stream  $\Delta a$  rises with time approximately linearly with distance along the stream, being strongest in the leading part of the stream, to which the sub-halo was closest as it approached the crossing point. Starting the sub-halo closer to the stream reduces the size of the pre-crossing  $\Delta a$  and the final asymmetry. Larger mass sub-halos do not lead to proportionally larger asymmetries. We conclude that the approximation of a straight line stream for the calculation of the velocity perturbations, which are then translated into the motions of a stream on a circular orbit does not capture all of the dynamics, but the approximation remains good in this case to a few percent.

For the warm stream the changes in epicycle sizes,  $\Delta a$ , are displayed in Figure 5. The perturbation induced epicycles are adding to pre-existing epicycles with random phases, hence there will be a spread from completely in-phase addition to out of phase subtraction. Figure 5 shows that the predicted relation and its negative largely bound the outcomes.

The evolution in time of the  $xy$  location of the particles in a cold stream simulation, effectively equivalent to the guiding centers of a warm stream, is shown in Figure 6. For this example we use a sub-halo of mass  $3 \times 10^6$  which increases the change in shape of the perturbed region with time. The stream starts with the shape of Figure 2, however with time the outer part falls behind the inner part. The characteristic sideways reversed “S” shape gradually becomes closer to a saw-tooth shape. Such shapes may be marginally visible in some current stream data (Carlberg & Grillmair 2013) and may become useful sub-halo detection signals in themselves as the quality of stream data improves to allow surface density measurements, not just linear densities along the stream.

### 3.3. Gaps in Streams

The development of the gap in the density of a stream according to Equations 12 and 13 is compared to a cold stream stimulation in Figure 7. The predictions does a very good job of describing the shape of the gap and its growth with time.

Warm streams have epicyclic motions which blur the density out along the stream which is not yet included in our cold stream analysis. Figure 8 shows the outcome of the same small impact parameter encounter as in Figure 7 but now on a warm stream of width 70 pc. The cold stream prediction (dotted line) does not do a very good job. However, we modify the prediction by sim-

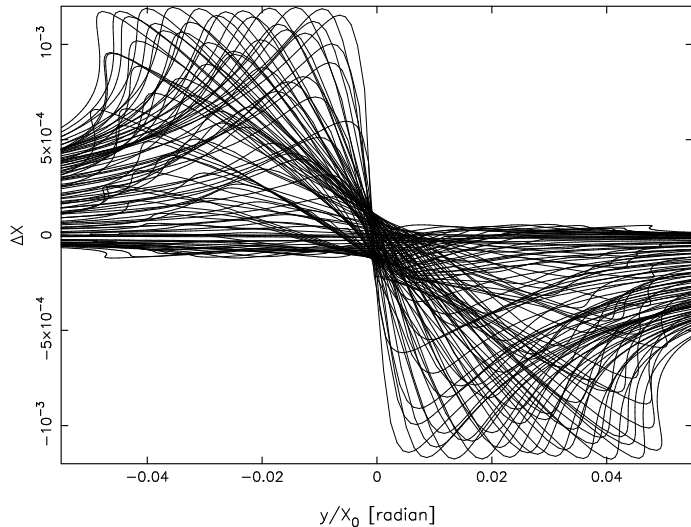


FIG. 6.— The evolution with time of the  $xy$  location of particles in a cold stream after a  $3 \times 10^6 M_\odot$  object passes through. The initial time has the shape of Figure 2 and the late times become saw-tooth shaped. Note that the  $x$  scale is greatly magnified relative to the  $y$  scale. The stream is shown every 0.8 units of time (about 1/8 of an orbital period) for 100 times. Line segments are drawn between a subset of the simulation points.

ply convolving the predicted density distribution with a Gaussian. The spread  $\sigma$  of the Gaussian is related to the FWHM of the stream multiplied by 1.414/2.355 where the factor of 1.414 allows for the fact that the epicycles along the stream are larger than their perpendicular size in the ratio  $2\Omega/\kappa$ , which is  $\sqrt{2}$  for a flat rotation curve, and, the factor 2.355 converts from FWHM to a Gaussian width.

We compare the gap measurements to the predictions for a 70 pc wide stream in Figure 8. The cold stream prediction (dotted line) gives a deeper and sharper gap than is found in the simulation (solid line). The velocity dispersion allowance does quite a good job predicting the shape of the gap (dashed line). Figure 9 shows a stream of width 150 pc where the width corrected prediction of the overall shape remains qualitatively correct, but a significant asymmetry is developing and the predicted depth is greater than measured. Not shown is a 300 pc wide stream, 1% of the orbital radius, which continues the trend of increasing discrepancy from our predictions with increasing stream width. The most significant error is that the depth is measured to be 0.5 to 0.6 of the mean level, whereas the predictions go nearly to 100% depth. The prediction continues to provide a useful estimate of gap width, but does not give an accurate density profile.

### 3.4. The Effect of Shear in Streams

The individual stars in stellar streams are drawn out from their progenitor objects with a range of angular momenta and radial velocities (Yoon, Johnston & Hogg 2011; Eyre & Binney 2011) which together fix the width of the stream. Both the angular momentum and the radial action,  $J_r = \kappa a^2$  are conserved quantities in an axisymmetric potential, which applies once the stars are away from the progenitor object. Progenitors that lose stars through a fairly well collimated outflow through

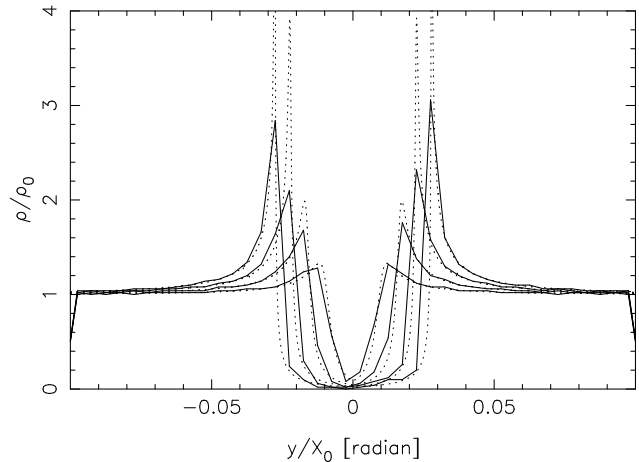


FIG. 7.— The line show the development of a density gaps in a nearly completely cold stream vs the angular coordinate after an encounter with a  $10^6 M_\odot$  sub-halo at dimensionless times 20, 40, 60 and 80, where the rotation period is  $2\pi$ . The dotted lines show the predicted relation at different times.

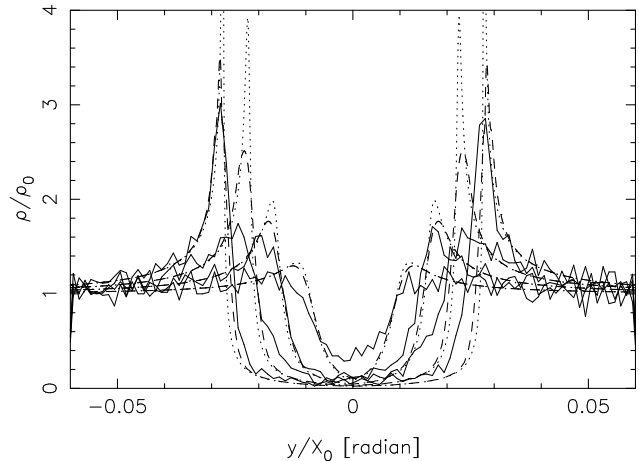


FIG. 8.— Same as Figure 7 except for a warm stream of width 70 pc. The dashed line shows the effect of adding in the epicyclic smoothing of the stream width along the stream.

the Lagrange points will have stream that are largely  $J_r$  dominated, with relative little shear (Küpper et al. 2008, 2012; Eyre & Binney 2011).

If there is significant range of angular momentum in the stream then it will cause gaps to shear with time so that any one-dimensional measure will see a decreased gap density once the tilt of the gap exceeds the gap width. The spreading of the gap into a tilted stripe along the stream and the consequent reduction of the depth at any location is straightforward to calculate. However, a useful prediction needs to have some way to estimate the range of angular momentum that is likely to be present. Such a prediction requires full n-body simulations that take into account the details of how the progenitor dissolves as it orbits in the potential of its host galaxy, which is beyond the scope of this paper.

A simple calculation shows when shear becomes an important effect. For illustration we assume that in a 60 pc wide stream half of the width at the origin of the stream is due to angular momentum (Eyre & Binney 2011). In

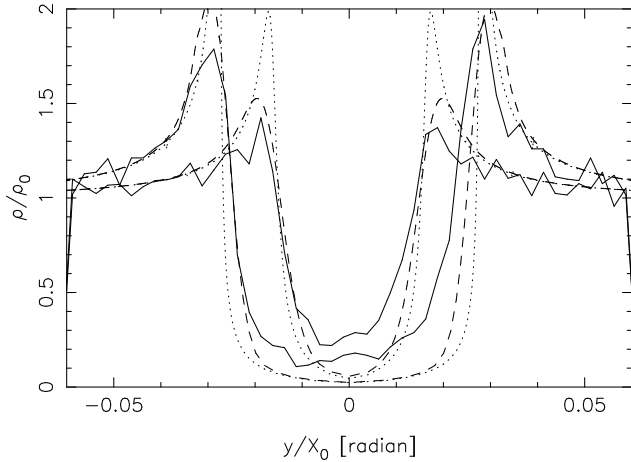


FIG. 9.— Same as Figure 7 except for a warm stream of width 150 pc. The dashed line shows the effect of adding in the epicyclic smoothing of the stream width along the stream. For clarity only the times 40 and 80 are plotted and the vertical scale has been reduced.

this case the range of angular momentum relative to the mean is 0.001 at 30 kpc orbital radius. Since small gaps are blurred out by the velocity dispersion in the stream, we consider the evolution of a gap having a length twice the width of the stream, 120 pc, 0.004 times the orbital radius. The stream shear in this case will reduce the density contrast in this gap to about half its initial depth in the time it takes the low and high end of the angular momentum in the stream to rotate apart by about twice the initial width of the gap. That time is 2 times the initial gap width divided by the fractional shear, or,  $2 \times 0.004/0.001$  which is 8 units of time, or about 1.3 rotation periods, which at 30 kpc is about 1 Gyr. The range of angular momentum spread diminishes linearly with distance down the stream, so at half the stream length the gap would take 2 Gyr to diminish to half its depth. Wider gaps would blur out over times directly proportionally to their length, so a gap ten times the stream width half way down the stream would last 10 Gyr. The simulations of dissolving globular clusters by

Küpper et al. (2008, 2012) suggest that the angular momentum range in those cases may be so small that angular momentum smearing is not a significant effect. We emphasize that the range of angular momentum relative to the radial action in the stars lost through the tidal lobes has not been extensively studied and the question of how both shear and substantially elliptical stream orbits effect the visibility of gaps remains to be resolved.

#### 4. DISCUSSION AND CONCLUSIONS

This paper provides a first order dynamical analysis of the velocity changes and subsequent development of a gap in a star stream after a massive object passes. A gap with a length comparable to the stream width will be blurred out through the subsequent orbital motions within the stream. Gaps that survive need to be 2 to 5 times the stream width, depending on details of the orbit and how stars are unbound from the progenitor object. The theory provides useful quantitative predictions for the resulting development of gaps in a stream, provided that the stream width is less than about 1% of its mean orbital radius. The numerical model can be used to make predictions of gap shapes in a variety of orbital situations. One insight is that although the single shape approach to gap-filtering developed in Carlberg et al. (2012); Carlberg & Grillmair (2013) is a reasonable approximation, the density profile gaps vary widely in their sharpness of shoulders.

The limitation of this study is that we study circular stream orbits and the details of the angular momentum, radial action and phase angle distributions of stars once unbound from the progenitor system is not yet sufficiently well understood in general situations to be incorporated into the model. Those details have an important influence on the real space appearance of streams and are the focus of ongoing studies.

This research was supported by CIFAR and NSERC Canada. An anonymous referee and Wayne Ngan provided comments that have strengthened and clarified the paper.

#### REFERENCES

- Angulo, R. E., Hahn, O., & Abel, T. 2013, arXiv:1304.2406  
 Benson, A. J., Farahi, A., Cole, S., et al. 2013, MNRAS, 428, 1774  
 Binney, J., & Tremaine, S. 2008, Galactic Dynamics: Second Edition, Princeton University Press  
 Barkana, R., Haiman, Z., & Ostriker, J. P. 2001, ApJ, 558, 482  
 Bode, P., Ostriker, J. P., & Turok, N. 2001, ApJ, 556, 93  
 Carlberg, R. G. 2009, ApJ, 705, L223  
 Carlberg, R. G. 2012, ApJ, 748, 20  
 Carlberg, R. G., Grillmair, C. J., & Hetherington, N. 2012, ApJ, 760, 75  
 Carlberg, R. G. & Grillmair, C. J. 2013, ApJ, 768, 171  
 Dehnen, W., Odenkirchen, M., Grebel, E. K., & Rix, H.-W. 2004, AJ, 127, 2753  
 Diemand J., Kuhlen M., Madau P., 2007, ApJ, 667, 859  
 Eyre, A., & Binney, J. 2011, MNRAS, 413, 1852  
 Johnston, K. V. 1998, ApJ, 495, 297  
 Johnston, K. V., Sackett, P. D., & Bullock, J. S. 2001, ApJ, 557, 137  
 Johnston, K. V., Spergel, D. N. & Haydn, C. 2002, ApJ, 570, 656  
 Ibata, R. A., Lewis, G. F., Irwin, M. J., & Quinn, T. 2002, MNRAS, 332, 915  
 Küpper, A. H. W., MacLeod, A., & Heggie, D. C. 2008, MNRAS, 387, 1248  
 Küpper, A. H. W., Kroupa, P., Baumgardt, H., & Heggie, D. C. 2010, MNRAS, 401, 105  
 Küpper, A. H. W., Lane, R. R., & Heggie, D. C. 2012, MNRAS, 420, 2700  
 Navarro, J. F., Frenk, C. S., & White, S. D. M. 1997, ApJ, 490, 493  
 Schneider, A., Smith, R. E., & Reed, D. 2013, MNRAS, 1489  
 Siegal-Gaskins, J. M., & Valluri, M. 2008, ApJ, 681, 40  
 Springel, V. et al. 2008, MNRAS, 391, 1685  
 Stadel, J., Potter, D., Moore, B., et al. 2009, MNRAS, 398, L21  
 Yoon, J. H., Johnston, K. V., & Hogg, D. W. 2010, ApJ, 731, 58